Journal of Robotics and Control (JRC)
Volume 6, Issue 5, 2025
ISSN: 2715-5072, DOI: 10.18196/jrc.v6i5.27539

Advanced Modeling and Comparative Error Analysis of Photovoltaic Cells Using Multi-Diode Models and EQE Characterization

Azem Hysa [1], Stela Sefa [2], I. M. Elzein [3*], Alfian Ma'arif [4], Mohamed Metwally Mahmoud [5*], Ezzeddine Touti [6*], Ali M. El-Rifaie [7], Noha Anwer [8]
[1] Department of Applied and Natural Sciences, "Aleksander Moisiu" University, Neighborhood 1, Currilave Street, Durres, 2001, Albania
[2] Department of Engineering and Marine Sciences, "Aleksander Moisiu" University, Neighborhood 1, Currilave Street, Durres, 2001, Albania
[3] Department of Electrical Engineering, College of Engineering and Technology, University of Doha for Science and Technology, Doha P.O Box. 2449, Qatar
[4] Department of Electrical Engineering, Universitas Ahmad Dahlan, Yogyakarta, Indonesia
[5] Electrical Engineering Department, Faculty of Energy Engineering, Aswan University, Aswan 81528, Egypt
[5]Applied Science Research Center, Applied Science Private University, Amman, 11931, Jordan
[6] Center for Scientific Research and Entrepreneurship, Northern Border University, Arar 73213, Saudi Arabia
[7] College of Engineering and Technology, American University of the Middle East, Egaila 54200, Kuwait
[8] Electrical Power and Machines Eng. Dept., The High Institute of Engineering and Technology, Luxor, Egypt
Email: [1] azemhysa@gmail.com, [2] stelasefa@gmail.com, [3] 60101973@udst.edu.qa, [4] alfian.maarif@te.uad.ac.id, [5] Metwally_M@aswu.edu.eg, [6] esseddine.touti@nbu.edu.sa, [7] ali.el-rifaie@aum.edu.kw, [8] nohaanwer69@yahoo.com
*Corresponding Author

***Abstract*—The consumption of electricity is substantially increasing as the striving of finding low carbon source of energy like solar energy. Through this research a consideration of three models to be addressed, SDM, DDM, and TDM, to extensively studying the functioning of PV cells. The objectives of the study are set to include plotting I-V and P-V characteristics, power output analysis over time, the calculation of energy accumulation and errors, as well as relative and absolute errors in I-V. The paper also determines the RMSE and analysis of the EQE of silicon, organic, perovskite and quantum dot PV cells. Mathematical analyses are used to solve nonlinear equations and applied simulation is adopted using MATLAB. The result provided an insight towards the electrical behavior of the PV cell at different conditions, demonstrating how external and model variables impact them. This class of information is vital for understanding physics, renewable energy and aid towards creating the precise analysis of PV cell function through the optimization of PV technology. The research also addresses critical issues such as energy conversion in PV systems, and error analysis.**

Keywords—Efficient Energy; Error Analysis; External Quantum Efficiency; PV Cells; Sustainability.

List of abbreviations

PV: Photovoltaic

PVCs: Photovoltaic cells

SDM: Single-diode model

DDM: Double-diode model

TDM: Three-diode model

I-V: Current-voltage

P-V: Power-voltage

RMSE: Root means square error

EQE: External quantum efficiency

RESs: Renewable energy sources

MPP: Maximum power point

EVs: Electric vehicles

V2G: Vehicle-to-grid

PSO: Particle Swarm Optimization

GA: Genetic Algorithms

ABC: Artificial Bee Colony

NRM: Newton-Raphson method

NRMC: NRM convergence

SMC: Secant method convergence

FPIC: Fixed-point iteration convergence

IQE: Internal quantum efficiency

SM: Secant Method

FPI: Fixed-Point Iteration

Rs: Series resistance

Rsh: Shunt resistance

FG: First generation

SG: Second generation

TG: Third generation

SR: Solar irradiance

Voc: Open circuit voltage

Isc: Short circuit current

I. INTRODUCTION

The PV outcome was first detected in 1839 by Becquerel; this essentially set in place the underlying principles for solar technology as we know it today [1]-[3]. What more contemporary reviews say is that Becquerel's early experiments already suggested the fact that photocurrent increases with light intensity [1], [4], [5]. A historical analysis indicates that the photoconductive nature of selenium was first reported by Smith in 1873 [1], [4]. Follow-up work by Adams and Day in 1876 demonstrated the direct generation of electric current from sunlight without mechanical parts [1], [6]. By 1883, Charles Fritts had fabricated the first working selenium PVCs, an achievement cited as the origin of practical PV devices [1]. A PVC is the fundamental building block of every PV system [7].

Modern studies describe PVCs as large-area semiconductor junctions that convert incident photons directly into electrical power [4]. Because this process is silent, emissions-free, and highly scalable, recent market analyses report accelerated adoption of PV for both residential micro-generation and utility-scale plants worldwide [8], [9]. To predict device behavior, researchers still rely on equivalent-circuit models; among them the SDM and the DDM remain the most broadly employed [4], [7]. The SDM is popular because it requires only five parameters and integrates easily into commercial simulation platforms [7], [10]. In the SDM, a current source representing the photogenerated charge carriers is placed in parallel with a diode and a shunt resistance, sometimes augmented by a series resistance for better accuracy [7]. Recent work has refined the SDM to improve accuracy under varying irradiance and temperature, yielding error reductions below 1 % on real I–V data [10].

RESs encompass various technologies including solar, wind, hydro, and geothermal systems [4]. Traditional electricity supply methods, such as hydroelectric or thermal power plants, often introduce disturbances in voltage and frequency that impact power quality for end users [11]. To address such challenges and to promote cleaner energy alternatives, PV technology has emerged as a viable and increasingly adopted solution [4], [12]. Among all RESs, PV energy is considered to have the highest potential due to its abundance and scalability in electricity generation [12].

PV systems require accurate modeling to optimize performance under varying environmental conditions. Due to its simplicity, the SDM remains widely employed. Other models, more advanced in incarnation, have been proposed to capture non-ideal characteristics of PVCs with greater accuracy: the DDM and the TDM [7]. Such models are very much required to build up the electrical behavior of solar cells and then for better energy conversion performance [7].

Simulation-based modeling with different physical and environmental parameters allows power electronics engineers to predict PV system behavior with greater reliability [10]. Numerical simulation methods, especially those using MATLAB® environments (temperature, and irradiance) have been the recent target of improvement for system analysis and evaluation of performance (I–V and P–V, series resistance, and diode quality factor) [13].

Programming complexity stands out as one major challenge faced by these methods. For instance, using a combination of MATLAB® scripts and C-language routines increases difficulty for users lacking programming expertise [14], [15]. To improve accessibility, recent efforts have focused on MATLAB®-only implementations where the PVC behavior is modeled using fundamental mathematical equations [10]. Functions developed by researchers such as González and Oi have enabled calculation of module current based on voltage, solar irradiance, and temperature input data [13], [16]. By fixing one parameter—either irradiance or temperature—it is possible to produce characteristic I–V and P–V curves and determine the MPP using additional script-based algorithms [10], [16].

Urban deployment of RESs, however, presents technical challenges. For instance, shading from buildings affects PV panel efficiency, and airflow obstructions reduce wind energy harvesting potential [17], [18]. In these environments, electricity is typically not supplied directly from generation units to end-users but is mediated through energy storage systems such as batteries. In this context, high-voltage batteries from EVs can serve as buffer storage units, enabling more dynamic energy management [19], [20].

Forecasts by international energy organizations estimate that by 2030, the global number of EVs could reach approximately 160 million units [21], [22]. This rapid expansion supports the concept of V2G networks, where EVs function as distributed energy storage resources. Such a system can enhance grid stability and flexibility in urban power infrastructure [23]. Nevertheless, realizing this potential necessitates the deployment of smart charging stations that can manage bidirectional power flow between EVs and the city's power grid [24].

The integration of RESs is becoming increasingly critical for ensuring sustainable energy supply in urban infrastructures [25], [26]. Despite this progress, these technologies still expression tasks in terms of efficacy and reliability, particularly in urban environments [27]. One promising approach to enhance system performance is through the deployment of EVs, which can serve not only as transport solutions but also as mobile energy storage units capable of accumulating and transferring surplus energy back to the city grid [28].

The implementation of V2G systems requires the development of smart charging infrastructure capable of supporting bi-directional power flow and intelligent load management [24]. However, most current research on charging infrastructure tends to focus on optimizing the spatial location and density of charging stations, often based on socioeconomic modeling and behavioral assumptions of EV users [29]. While this is valuable, it overlooks the dynamic energy-balancing potential of distributed EV fleets and their strategic integration into urban power systems [30].

The number of grid-connected PV plants, including those with integrated battery storage systems, continues to rise annually in many countries due to policy incentives and declining technology costs [31], [32]. In 2021, Germany led the European solar market by adding 5.3 GW of new PV capacity, followed by Spain (3.8 GW), the Netherlands (3.3

GW), Poland (3.2 GW), and France (2.5 GW), reflecting a broad continental push toward renewable deployment [33].

The classification of PVCs is commonly based on technological factors, material composition, structural design, and generation types [34], [35]. According to generational categorization, PV technologies are divided into three primary groups FG\ SG\ TG [36]. FG encompasses silicon-based technologies, including monocrystalline and polycrystalline silicon PVCs, which dominate the commercial market due to their stability and efficiency [37]. The SG typically includes thin-film technologies such as a-Si, CdTe, and CIGS, offering lower material usage and flexibility advantages [38], [39]. The TG introduces more advanced concepts, such as perovskite PVCs, organic PVs, quantum dot PVCs, and dye-sensitized PVCs, all aiming to push the efficiency-cost boundary of traditional technologies [40], [41].

PVCs offer numerous advantages, including low environmental impact during operation, low maintenance requirements, and potential for reducing electricity bills, while also increasing property value [42], [43]. However, several drawbacks remain, such as the relatively non-green nature of some manufacturing processes, high initial capital costs, the necessity for power inverters, and intermittent energy production due to PVCs dependency [44], [45].

In 2020, Oxford PV developed a hybrid perovskite-silicon tandem cell that surpassed 29% power conversion efficiency, marking a significant advancement in the field [46], [47]. Recent studies suggest that even higher efficiencies could be achieved through integration of nanostructures such as silicon nanowires, nanotubes, and novel materials like organic dyes and conductive polymers, especially within the context of third-generation solar cells [48], [49]. Although lab-scale devices have reached efficiencies of up to 47.1% under concentrated light, these technologies are still in early research and have yet to reach commercial viability [50].

This paper begins by outlining the essential characteristics of PVCs. Following that, the temporal energy and power output of various PV technologies is presented graphically, highlighting system performance dynamics [51]. A subsequent section focuses on numerical analysis through the implementation of iterative techniques commonly applied in PV energy modeling. By considering a nonlinear function g(x), its roots are explored graphically using the NRM, the SM, and FPI [52].

Lastly, three mainstream models of equivalent circuit of PVCs are introduced: The SDM, DDM, and TDM. Both models hold varying concentrations of physical phenomena including recombination and leakage losses, and they must be wise to depict solar energy systems exactly and wisely in relation to their performance prediction and simulation accurately [53].

This paper provides a critical examination of behavior of PVCs through three of the commonly deployed modelling methods: The SDM, the DDM and the TDM. I- V and P- V parameters are tested under different environmental, electrical conditions such as Rs, Rsh, PVCs temperature, and irradiance of sun rays. These parametric manipulations give profound understanding of nonlinear response of PVCs their performance at real situations in which its works can be simulated and compared between theoretical conditions and those faced in the real situation where the PVCs are stressed.

One of the new contributions of the work is the quantitative measure of absolute error in terms of the character of expected and actual I-V and P-V for the three models. The output of graphical output is the use of plotting absolute error versus voltage plots and real-time monitoring of actual and theoretical power output and it gives vital validation figures of model fidelity. Moreover, upon visualizing and comparing dynamic output performance in all three different models not only does the paper reveal constraints of simplified modeling structures such as SDM to recombination and leakage effects, but it also demonstrates the greater accuracy of using DDM and TDM at yielding dynamic output in response to changing environmental conditions.

This study can eventually be interpreted as the asset of analyzing the behavior of high resolution and accuracy of PVCs. It assists engineers, researchers, and system designers in the choice of PV models as well optimize them in order to be used in simulating, forecasting the performance of system and control of power electronics in real time, particularly those that involve uncertainties of the environment.

II. METHODS

A wide array of computational methodologies has been proposed and utilized for modeling PVCs, typically classified into direct and indirect techniques [32]. Indirect methods include heuristic and metaheuristic algorithms such as PSO, GA, and ABC, which are widely used for estimating key parameters like the five, seven, or eight-parameter models of PVCs [54], [55]. On the other hand, direct methods, such as Newton's method, are extensively applied in engineering and mathematical contexts to solve nonlinear systems of equations, including those emerging from PV modeling [56], [57].

Nonlinear functions, often denoted as g(x), naturally arise in the modeling of I–V characteristics of PV panels, regardless of whether the SD, DD, or more complex equivalent circuit models are used [58]. These nonlinear functions encapsulate physical behavior such as diode recombination and series/shunt resistance effects, and are often difficult to solve analytically [59]. In this context, computational modeling becomes critical, allowing the simulation and optimization of PVCs behavior under varying irradiance and temperature conditions [60].

To accurately solve such nonlinear equations, iterative numerical methods are preferred. Among them, NRMC, SMC, and FPIC stand out for their convergence capabilities in solar modeling tasks [61]. From a wide selection, in particular, NRMC remain the most popular iterative method owing to its quadratic convergence and easy implementation for nonlinear transcendental functions [62]. The I–V and P–V relationships in the SD–PVC equivalent system is obtained from an implicit nonlinear transcendental equation. Analytical solution almost never exists for such an equation,

thereby drawing the focus of numerous numerical solution procedures that have been developed to solve it efficiently [63]. Among the many methods proposed, the NRMC being the popular one, due to its high convergence rate whenever the first approximation lies sufficiently near the actual root [64]. This iterative methodology is capable of being employed in almost any area of engineering and thus has justifiably come to be considered one of the best solutions to modeling problems of a PV nature [64].

The NRMC is a popular method for numerically solving the nonlinear equations due to their property of fast convergence if certain requirements are fulfilled [65]. When an initial estimate is provided nearby the root, the sequence generated by the iterative procedure tends to converge to the best root for the function [66]. Mathematically, NRMC can therefore be expressed by the recursive formula [67]:

$$x_{k+1} = x_k - \frac{f(x_k)}{f'(x_k)} \quad (1)$$

where, x_{k+1} is the k^{th} iteration root estimation update, $f(x_k)$ evaluation function at x_k, and $f'(x_k)$ is its derivation at that point.

This expression is applied repeatedly until $|f(x_{k+1})|$ becomes sufficiently close to zero, indicating convergence of the root estimate [68]. The method's simplicity and rapid convergence make it a preferred choice for solving nonlinear models in engineering and scientific computations, including PVC modeling and optimization tasks [69].

Another iterative method that is used is the SMC. This method, unlike the NRMC, is used in cases where the first derivative cannot be easily determined by the NRMC. So, this is a simpler method through which the first derivative is first approximated. The SMC can be determined from two preliminary estimates. This iterative method approximates the derivative using the difference coefficient [70]:

$$x_{k+1} = x_k - f(x_k)\frac{x_k - x_{k-1}}{f(x_k) - f(x_{k-1})} \quad (2)$$

While the iterative fixed-point method is applied to equations of the form $x = g(x)$:

$$x_{k+1} = g(x_k) \quad (3)$$

This is also an iterative method that is widely used. In this case, we can iterate until the error is at such a threshold. In these iterative methods it is important that the function $g(x)$ be rearranged in a form appropriate for the respective method in order to get the solution as close as possible to the true value with a small error. Consider a polynomial function of g such that [71]:

$$g(x) = x^3 - 6x^2 + 11x - 6 = 0 \quad (4)$$

This is a nonlinear equation that we want to solve iteratively because this function does not have an exact analytical solution. For the FPIC, the function $g(x)$ should be rearranged to a form suitable for the method. Fig. 1 shows the solution of a given function with three different numerical methods, as follows: Fig. 1(a) - (NRMC), Fig. 1(b) - (SMC), and Fig. 1(c) - (FPIC). Finally, we emphasize the fact that g-functions are related to a specific problem, such as a nonlinear equation that describes the nonlinear dynamic behavior of PVCs, as we will see later in this study. Therefore, the study, analysis, and solution of these functions is very important for science and engineering as well as many other fields such as medicine, economics, etc.

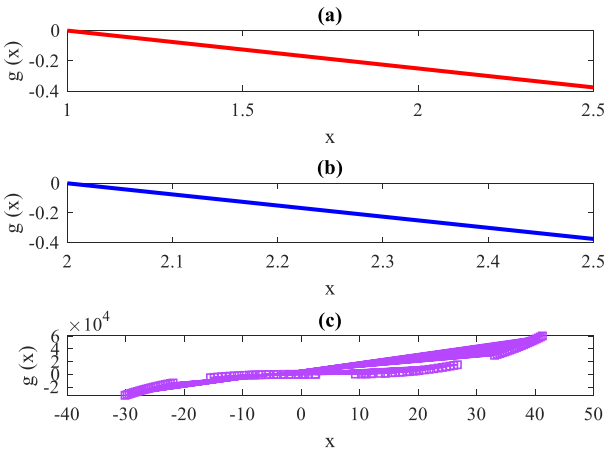

Fig. 1. (a) NRMC, (b) SMC, (c) FPIC

Several recent studies have introduced various mathematical models to analyze the electrical behavior and output characteristics of PVCs [72]. These models aim to represent the I–V and P–V relationships under diverse operational situations [73]. The most commonly adopted models include the SDM, which simplifies the PVC into a basic equivalent circuit entailing of a current source, diode, Rs, and Rsh [74]. The DDM adds an extra diode to improve accuracy in the low-voltage region [75]. Meanwhile, several physical models are able to simulate devices, whereas at the circuit level, models such as SPICE allow for simulating PV systems at a fairly general level, including simulation coupled with power electronics [77], [78]. The modified SD model usually also goes by the many-names one of the "five-parameter" method for practical variation of accurately fitting experimental data and improving parameter extraction [79]. The increased level of mathematical complexity, however, renders it less favored in routine simulation tasks than simpler models with which it would usually be compared, such as the basic SDM or DDMs [80]. Another alternative includes utilizing detailed physical models based upon semiconductor theory that provide insights into charge carrier recombination, optical losses due to reflection and transmission, and temperature-dependent effects in PVCs [81]. These physical models offer a more detailed understanding of intrinsic behavior than the approximations given by circuit-level representations [82].

By the same token, empirical modeling techniques have recently been supported and stressed by many researchers. Setting up equations that are predictive usually implies the use of polynomial or exponential functions given the few resources available for measuring only I-V characteristics and possibly environmental variables such as irradiance and temperature [83].

On the other hand, it is widely held that the SPICE-based circuit modeling approach to PV simulation and optimization is the best, allowing electronic engineers the capability to

simulate the dynamics of PV modules under either load or operating conditions.

Conversely, these models seek to reproduce the electrical behavior of PV systems through the use of equivalent circuit representations such as single-diode or double-diode models [85]. SPICE-based implementations permit the exact simulation of performance variations in the PV system due to environmental changes like irradiance and temperature [86]. Moreover, SPICE simulations provide a means for investigating dynamic responses under fluctuating load conditions, thereby making them an essential tool in system-level PV design and reliability studies [87], [88].

There has always been a necessity to consider a three-parameter model because of its balance in computational efficiency and accuracy when simulating I–V characteristics of PV modules." The model's ability finally rests upon the method employed for estimating unknown parameters, mostly considered to be photo-generated current (I_{ph}), saturation current of diode (I_0), diode ideality factor (n), R_s, and R_{sh} [90]. A wealth of analytical and numerical methods has been purposed to accurately estimate these parameters, depicting the vast attention received by these parameters [91]. Some authors use iterations in which R_s and R_{sh} are adjusted until satisfying the condition that the result from the model converges with the experimental data, indicating a strong predictive capability [92]. This may perhaps use initial guesses taken from slopes of the I–V curve at V_{oc} and I_{sc}, which are usually furnished in datasheets [93]. Experimental validation with mono-crystalline silicon (Mono-Si) modules has shown excellent correlation between simulated and measured performance, hence supporting the model's robustness [94]. The SDM can be categorized into five, four, or three-parameter variants, all based on a single exponential term [95]. The five-parameter model includes all standard parameters, while the four-parameter version assumes infinite shunt resistance (neglecting R_{sh}) [96]. The three-parameter model simplifies further by assuming both zero series resistance and infinite shunt resistance, eliminating both R_s and R_{sh} from consideration [97]. On the other hand, the DDM adds complexity with six unknown parameters and two exponential terms, allowing it to better capture recombination losses in some cases [98]. However, both SDM and DDM require detailed parameter knowledge that is often not provided in manufacturer datasheets, necessitating parameter extraction methods [99].

The fundamental Shockley equation describes the I–V characteristic of an ideal PVC, modeling it based on semiconductor diode theory [100]. This equation is expressed as [101], [102], [103], [104]:

$$I = I_{ph} - I_d = I_{ph} - I_0 \left[\exp\left(\frac{qV}{\mathrm{a}k_BT}\right) - 1\right] \quad (5)$$

where I_{ph} - is the photocurrent generated by light absorption, and I_0 is the diode reverse saturation current. The term $I_d = I_0 \left[\exp\left(\frac{qV}{\mathrm{a}k_BT}\right) - 1\right]$- represents the current flowing through the diode under forward bias. Here, a a denotes the diode ideality factor, which adjusts the exponential term to reflect recombination losses in real devices. The voltage V is measured across the diode terminals, and the constants, $k_B = 1.381\times10^{-23}\ J/K$ (Boltzmann constant) and $q = 1.602\times10^{-19}\ C$ (electron charge), are fundamental physical constants. The temperature T is the junction (operating) temperature, typically measured in Kelvin.

When modules are connected in series, the output voltage increases proportionally to the number of series-connected cells N_s, while parallel connections increase the output current [105]. However, this ideal equation fails to capture the non-linear behavior of practical PV arrays, which are subject to resistive and thermal losses [106]. To accurately represent the terminal characteristics of a real PV module or array, two parasitic resistances must be introduced into the equation: the series resistance (R_s) and the shunt (parallel) resistance (R_{sh}) [107]. These parameters reflect ohmic losses due to contacts, wires, and leakage currents across the junction, respectively [108]. The modified SDM equation becomes [109]:

$$I = I_{ph} - I_0 \left[\exp\left(\frac{q(V + IR_s)}{\mathrm{a}k_BT}\right) - 1\right] - \frac{V + IR_s}{R_{sh}} \quad (6)$$

This extended form improves the accuracy of PV module simulations and is widely employed in numerical models and MPPT control strategies. The series (R_s) and shunt (R_{sh}) resistances can be estimated from V–I curve as follows:

$$R_s = -\frac{dV}{dI} - \frac{V_{Tn}}{I_{sc}} \quad (I = 0, V = V_{oc}) \quad (7)$$

$$R_{sh} = -\frac{dV}{dI}\ (I = 0, V = V_{oc}) \quad (8)$$

The current passes the R_{sh} is given as:

$$I_{sh} = \frac{V+IR_s}{R_{sh}} \quad (9)$$

The DDM of a PVC extends the basic SDM by incorporating an additional diode to account for the recombination losses in the depletion region [110]. A more precise representation of the I–V chs., through this model is leveraged, and more particularly under the conditions of low SR [111]. The equation below describes the mathematical model of the PVC in relation to the DDM [112]:

$$I = I_{ph} - I_{01}\left[exp\left(\frac{q(V+IR_s)}{a_1k_BT}\right) - 1\right] - I_{02}\left[exp\left(\frac{q(V+IR_s)}{a_2k_BT}\right) - 1\right] - \frac{V+IR_s}{R_{sh}} \quad (10)$$

where; a_1 and a_2: Ideality factors of the 1st and 2nd diode.

The recombination current is captured by this modeling scheme [113]. It is normally used in simulation applications of photovoltaic performance, as well as the determination of experimental parameters [114]. To further improve modeling accuracy for PVCs under varied conditions, the TDM introduces an additional diode to account for more complex recombination and diffusion mechanisms [115]. This model is especially useful for high-efficiency or concentrator PVCs where multiple recombination pathways are present [116]. The current in the TDM is:

$$I = I_{ph} - I_{01}\left[\exp\left(\frac{q(V+IR_s)}{\mathrm{a}_1k_BT}\right) - 1\right] - I_{02}\left[\exp\left(\frac{q(V+IR_s)}{\mathrm{a}_2k_BT}\right) - 1\right] - I_{03}\left[\exp\left(\frac{q(V+IR_s)}{\mathrm{a}_3k_BT}\right) - 1\right] - \frac{V+IR_s}{R_{sh}} \quad (11)$$

Each diode in the model corresponds to a specific loss mechanism: diffusion, surface recombination, and space-charge region recombination [117]. While more complex, this model yields better accuracy for PVCs operating in non-ideal conditions such as low light or high temperatures [118]. However, because of the amplified number of parameters, the model requires sophisticated parameter extraction methods and fitting algorithms [119]. The models' effectiveness mentioned above is assessed by objective functions, specifically those pertaining to RMSE. So, another important aspect of mathematical models of the PVCs are two statistical indicators, absolute error and the RMSE as defined by [120]:

$$\varepsilon_{absolute} = |I_{measured} - I_{model}| \quad (12)$$

And

$$RMSE = \frac{1}{N}\sum_{i=1}^{N}\left(I_{i,measured} - I_{i,model}\right)^2 \quad (13)$$

These two metrics are used to evaluate the degree of precision of the applied mathematical model and the correctness of the suggested technique [121]. A common statistic for evaluating the average difference between expected and actual I-V or P-V data in PVC models is RMSE. Better agreement and more model fidelity are indicated by a lower RMSE [122]. During parameter estimation for PV models—such as SD or DD equivalents—many studies use RMSE minimization to fit model outputs to experimental I–V curves. Techniques like Archimedes optimization algorithm and other metaheuristic methods specifically optimize RMSE to improve parameter accuracy [123].

RMSE is especially crucial when comparing models under non-ideal or partial shading scenarios. Lower RMSE values help identify which model (e.g., SD- vs DD) better captures the real device behavior [124]. Recent research critiques the conventional RMSE calculation methods and proposes more exact analytical solutions—such as those based on the Lambert W function—to more accurately evaluate modeling error for PVCs [125]. Different RMSE-based fitting strategies—such as minimizing RMSE in (I) vs (V), or hybrid approaches (I&V)—can significantly impact the extracted parameters for parasitic resistances and diode ideality. These choices directly influence the RMSE and thus model reliability [126].

III. RESULTS AND DISCUSSION

In this study, original simulations were carried out using MATLAB® 2024b to obtain the I–V and P–V chs., of PVCs under varying physical and environmental parameters. The analysis focuses on how changes in diode IF (a), I_0, R_s, and R_{sh} affect the electrical behavior of PVCs. Additionally, realistic environmental conditions—such as different temperature values and SR levels—were incorporated in the simulation. The numerical computations and visualizations were fully implemented by the author in MATLAB®, a proprietary software developed by MathWorks, widely used in engineering and scientific research for numerical modeling and simulation. MATLAB® offers a robust environment for technical computing and graphical visualization, which facilitated the generation of high-resolution output plots.

Fig. 2 presents the simulated I–V and P–V chs., for varying values of Io and a, illustrating the effects of diode parameters on the PV module's output. The results are derived entirely from original code and parameter sets developed within this work, without reliance on external simulation templates or databases.

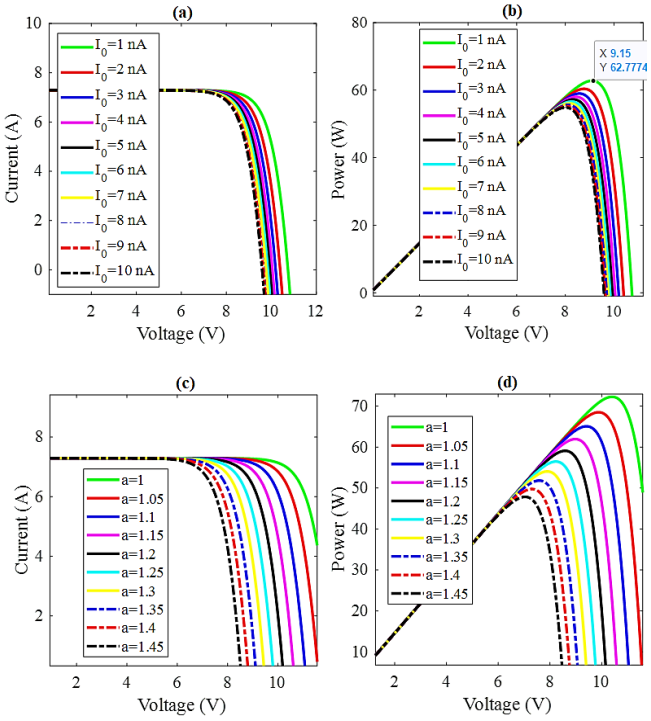

Fig. 2. (a) I-V curves for variation in I_0. (b) P-V curves for variation in I_0. (c) I-V curves for parametric difference. (d) P-V curves for parametric difference

I-V and P-V chs., under changing Io of the diode are exposed in Fig. 2(a) and Fig. 2(b). In this case, I_0 changes with ten values of 1 nA, 2 nA, 3 nA, 4 nA, 5 nA, 6 nA, 7 nA, 8 nA, 9 nA and 10 nA, respectively. Fig. 2 a and Fig. 2 b demonstrates how a greater diode Io results in a lower output power and voltage while maintaining the same current. The maximum value of the output power in this case is approximately 62.8 W/m^2 (see Fig. 2(b)).

Fig. 2(c) and d show I-V and P-V curves, respectively for ten different values of the ideality factor (IF) of the diode. The values used for the IF in this calculation are: 1, 1.05, 1.1, 1.15, 1.2, 1.25, 1.3, 1.35, 1.4, and 1.45. The diode's IF typically ranges from 1 to 2. The simulation findings in Fig. 2(c) and Fig. 2(d) show that the more the IF value was close to 2, the more power was extracted from the PVC. However, the simulation results with a=1.4 do not accurately represent the situation because the type of PVC with a high IF also exhibits high reverse Io, which would typically lead to low V_{oc}, making it practically impossible to obtain such a high value of V_{oc}. Monocrystalline silicon (Si) is represented by diode IF values between 1.1 and 1.3. In its case the lines shown in the graph with the colors blue, pink, black, cyan and yellow correspond to PVCs made of monocrystalline silicon material.

Values of a from 1.2 to 1.4 correspond to the material Polycrystalline Silicon (Si). So, the lines shown in the graph with the colors black, sky, yellow and the dashed lines in blue

and pink. Values of a from 1.1 to 1.2 correspond to the material CdTe (lines in blue, pink and black). To obtain the results shown in Fig. 2, we first determined the values of constants such as Boltzmann's constant, electron charge, nominal SC current (I_{scn}=8.1 A), nominal OC voltage constant (V_{ocn}=33 V), Temperature current constant (K_i=0.00322 K), No. of series connected PVCs (N_s=55), temperature (25 ºC).

Fig. 3(a) show the output power in watts over time per hour for a PVC. To obtain this result, we performed a numerical simulation in MATLAB in the case where temperature and SR change over time according to a sinusoidal law to mimic the typical variation over a day. So, the time is simulated over 24 hours, a typically day. The SR during a day varies from 0 to 1000 W/m^2 according to the law: $Irradiance = 1000\left|\sin\left(\frac{\pi t}{12}\right)\right|$ (Simple model: peak at noon). The temperature varies from 15 ºC to 35 ºC according to the sinusoidal law: $T = 25 + 10\sin\left(\frac{\pi t}{12}\right)$. To perform these calculations, the SDM was used. Fig. 3(b) illustrates the P–V chs., for ten different values of R_s. The results indicate that increasing R_s alters the slope of the corresponding I–V curves, which shifts the location of the MPP. As R_s increases, the output power of the PVC decreases due to higher resistive losses. The maximum output power obtained under the ideal case with R_s=0Ω is approximately 57 W, as shown in the plot. In a separate analysis, simulations were conducted for various R_{sh} values, specifically 0.05 Ω, 1 Ω, 10 Ω, 30 Ω, 70 Ω, and 1000 Ω. It was observed that higher shunt resistance enhances the output power of the PV cell. When the R_{sh} is low, the current decreases more abruptly near the short-circuit region, indicating greater leakage losses. The impact of R_{sh} on both I–V and P–V chs., is shown in Fig. 3(c) and Fig. 3(d), respectively [14].

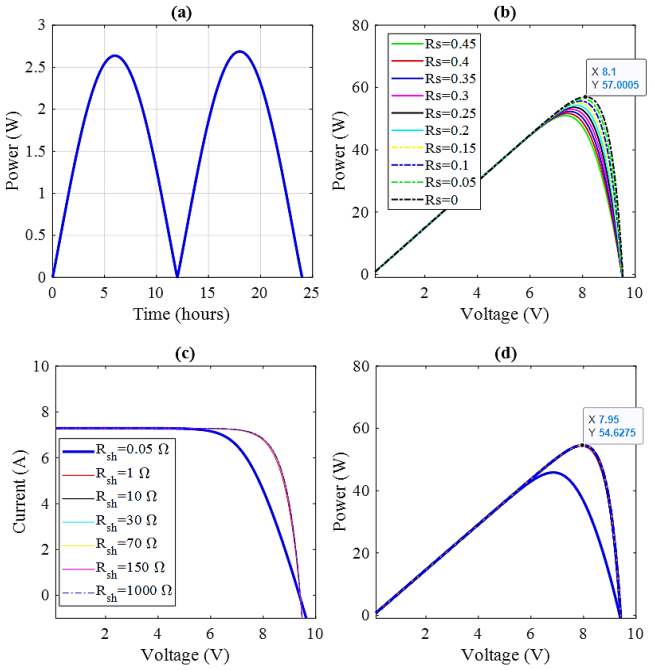

Fig. 3. (a) Power output of a PVC over time. (b) P-V curves for different R_s (SDM). (c) I–V curves for parametric variation of R_{sh} (SDM). (d) P-V curves different R_{sh} (SDM)

Fig. 4(a) and Fig. 4(b) show I-V and P-V chs., at different temperature (−20 ℃, −10 ℃ 0 ℃, 10 ℃, 20 ℃, 30 ℃, 40 ℃, 50 ℃, and 60 ℃), respectively with fixed SR =1000 W/m^2. The PVC's performance was noted to be best at 0 ℃. These findings indicate that PVC voltage exhibits a notable drop in value as temperature rises, whereas cell current likewise marginally increases. While the maximum power output drops, the Isc rises by a significantly smaller amount than the V_{oc} does.

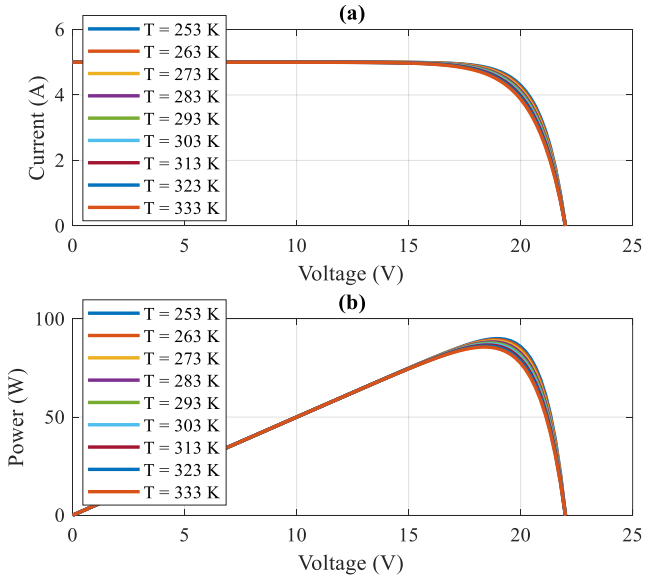

Fig. 4. (a) I–V chs., at different operating temperatures and constant SR based on the SDM. (b) P–V chs., at the same temperature variations and constant SR conditions with the SDM

Fig. 5(a) illustrates the I–V chs., of the SD- PV model under varying levels of SR, while the PVC temperature remains fixed at T = 25 °C. Correspondingly, Fig. 5(b) displays the P–V curves under the same thermal condition. The simulation results indicate that as the SR increases, both the output current and the maximum power of the PVC exhibit a noticeable increase. However, the voltage shows only a slight enhancement. This trend arises because the V_{oc} depends logarithmically on the SR, whereas the I_{sc} has a near-linear dependence on it. To perform this calculation, we used the SR values: 1500 W/m², 1800 W/m², 2000 W/m², 2500 W/m², 3200 W/m², 3500 W/m², 4700 W/m², 4750 W/m², 6000 W/m², 6030 W/m², 6500 W/m², and 6800 W/m². These SR values are typical for European countries such as Albania, Montenegro, Greece, etc. Using the same SR values, we have also performed calculations for the DDM and the I-V and P-V chs., for this model are presented in Fig. 5(c) and Fig. 5(d), respectively. Also, the other parameters we used for this calculation are the same as those of the SDM, for example the temperature is constant T = 25℃, I_{sc} = 5.1 A, V_{oc} = 0.6 V, Number of series cells, N_s = 1, R_{sh} = 101 Ohm, and R_s = 0.011 ohm. Comparing the result of Fig. 5(b) with that of Fig. 5(d) we see that for the same values of SR, the output power is lower in the DDM. For the DDM is used saturation current of first diode I_{01} = I_{sc}/(exp (V_{oc}/(2V_t))-1) and saturation current of second diode (lower) I_{02} = I_{01} / 100, where $V_t = kT/q$ – is thermal voltage in V.

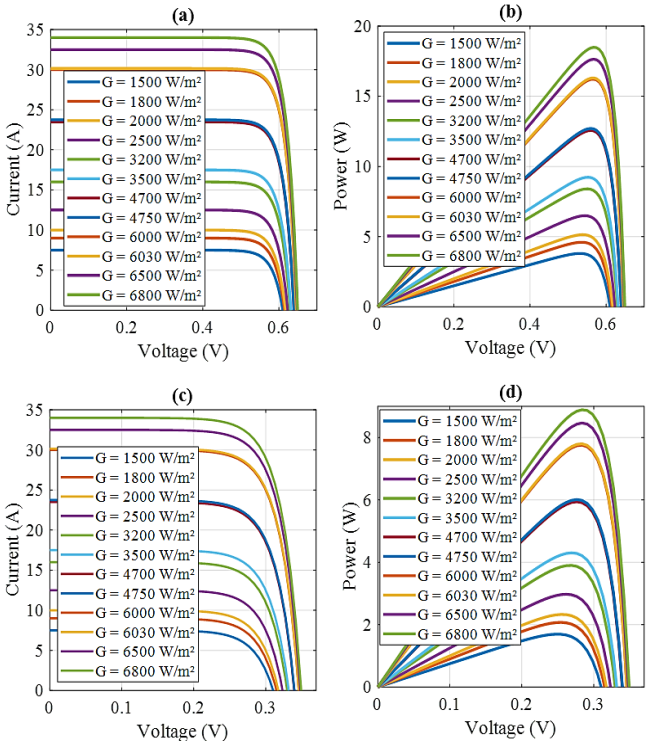

Fig. 5. (a) I-V chs., with SDM. (b) P-V chs., with SDM. (c) I-V chs., with DDM. (d) P-V chs., with DDM

For the TDM we used the parameters: photocurrent under standard irradiance (1000 W/m²) is I_{ph0} = 5 A, reverse saturation current of diode 1, diode 2 and diode 3 is $I_{s1} = I_{s2} = I_{s3} = 10^{-10}$ A, thermal voltage in V at 300 K, typical value for silicon is V_t = 0.026, R_{sh} (Ohms), high value indicating small leakage is R_{sh} = 1000, R_s in Ohms, small value assuming low losses R_s = 0.01, irradiance levels to simulate (in W/m²) are: 200 W/m², 400 W/m², 600 W/m², 800 W/m², 1000 W/m². The results of the I-V and P-V curves for the TDM at different SR levels are presented in Fig. 6(a) and Fig. 6(b), respectively.

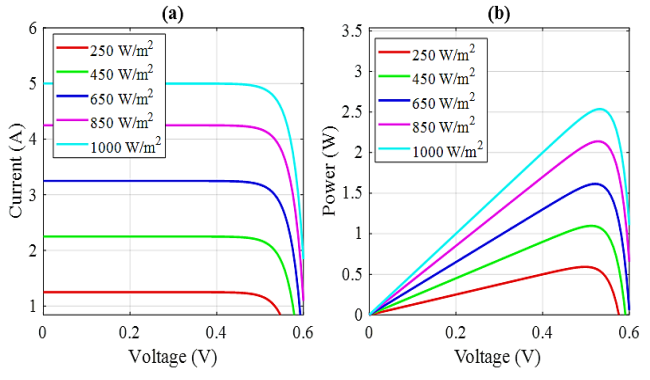

Fig. 6. (a) I-V curve for the TDM at different SR levels. (b) P-V curve for the TDM at different SR levels

PVCs can be bifacial and monofacial. Traditional PVCs that capture sunlight only from the front side are the monofacial PVCs. Monofacial PV panels are PVCs that generate electricity only from sunlight hitting the front side of the PVC. The back is usually covered with a dark material, meaning it does not contribute to power generation [127]. However, the PV panel can capture sunlight from both the front and back sides, increasing efficiency by using light reflected from various surfaces on the Earth or on the roofs of buildings. In this case, the solar cells are bifacial. Bifacial PVCs are designed to be hit by sunlight on both the front and back sides, thus increasing the total production of the necessary electrical energy [127], [128]. When compared to their monofacial counterparts, bifacial modules greatly increase energy yield by capturing light that is reflected from nearby surfaces and the dispersed components of sunlight. [129]. This characteristic is especially helpful in settings where ground reflectivity is high or in installations that use engineered ground cover to increase reflection [130]. Because bifacial cells are less expensive to produce than monofacial PVCs, PV module producers have started incorporating them into monofacial modules. This is primarily associated with a 65.3% decrease in the amount of back aluminum paste used, which results in a 0.5 cent/wafer cost reduction for M4 (161.7 × 161.7 mm^2) size wafers. [131].

Fig. 7 displays the I-V and P-V chs., of monofacial and bifacial PVCs under standard test conditions. To obtain these results, first defines voltage ranges and assumes different short-circuit currents for monofacial and bifacial PVCs. Define I-V chs., (using an ideal diode model approximation). The red curves represent the I-V and P-V chs., for monofacial PVCs and the blue curves represent the bifacial PVCs. This result helps visualize how bifacial PVCs perform better by capturing additional reflected light.

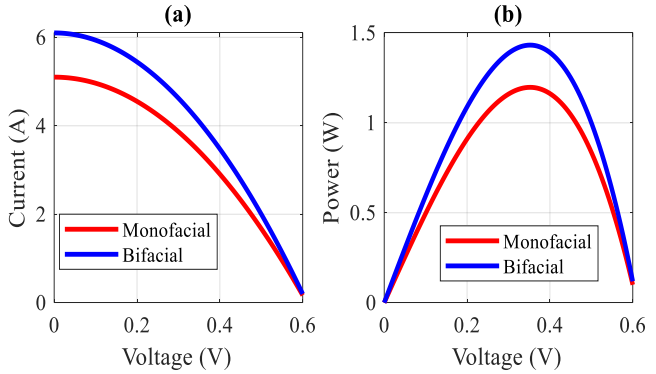

Fig. 7. (a) I-V chs., of PVCs (monofacial and bifacial). (b) P-V chs., of PVCs (monofacial and bifacial)

Fig. 8(a) show the power output of a PVC over time during a day (24 hours). From this result we see that the power output varies with time according to a sinusoidal law. The maximum output power in Watts is 300 W. Fig. 8(b) shows the energy of the PVC over time for 24 hours. Energy error over time for PVCs can be calculated. To make this calculation, the estimated energy output $E_{estimated}$ is compared with a measured actual energy E_{actual}. Energy error is $E_e = E_{estimated} - E_{actual}$. Fig. 8(c) shows energy output over time. The blue curve represents Estimated energy over time and red curve represents actual energy over time. Relative error of energy is $E_r = \left|\frac{E_e}{E_{actual}}\right| 100\%$ (Percentage Error). Fig. 8(d) shows relative error (%) over time.

The absolute error of the electric current in amperes from the electric voltage in volts for the PVC can be graphically represented. Fig. 9 shows the absolute error for output I versus output V.

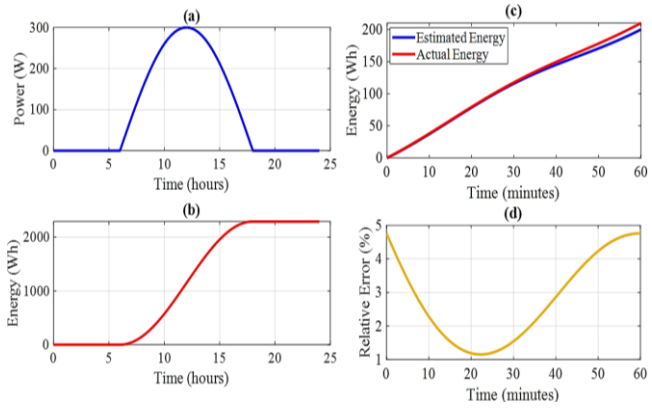

Fig. 8. (a) PVC power output. (b) PVC energy accumulation. (c) Energy output over time. (d) Energy error (relative error (%)) over time

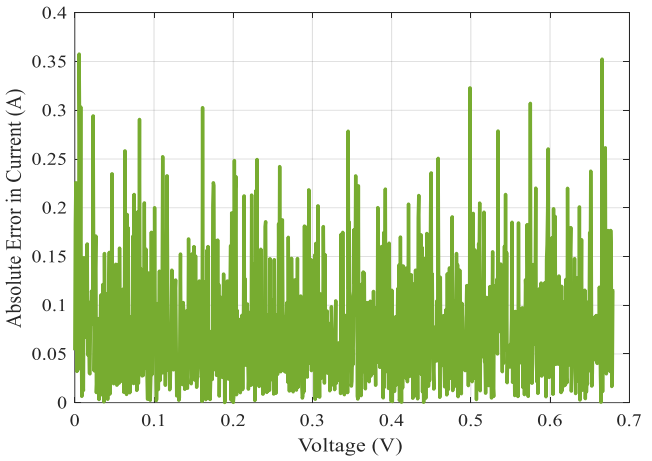

Fig. 9. Absolute error in I verses V for PVC

Fig. 10(a) shows actual power and expected power output in Watts verses time in hours. We can also plot the power error for the PVC over time. This result is shown in Fig. 10(b). The simulation time used in this calculation is 10 hours. This error in power is calculated as the difference between actual and expected power. Fig. 10(c) shows the I-V characteristic for the measured current (blue curve) and for the simulated current (red dashed curve). Fig. 10(d) shows the P-V curves for the measured power (blue curve) and for the simulated power (red dashed curve). The RMSE calculated for the I-V chs., is 0.1308, while for the P-V chs., this error is calculated to be 0.6636.

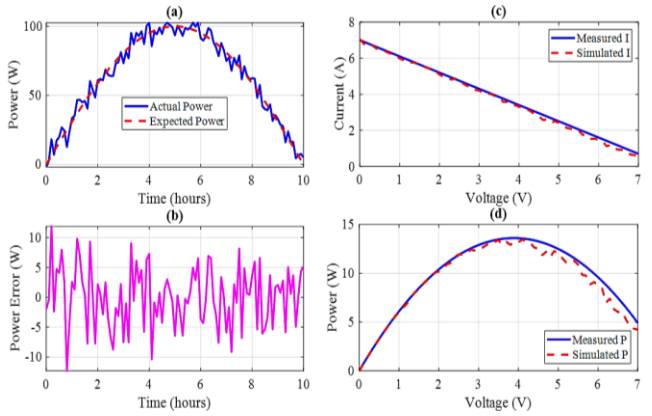

Fig. 10. (a) Actual and expected power output over time in hours. (b) Power error over time. (c) I-V curve (RMSE = 0.1308 A). (d) P-V curve (RMSE = 0.6636 W)

Fig. 11 shows absolute error I-V and P-V curve PVCs. To calculate and plot this error between the measured and simulated I-V and P-V curves of PVCs, we compare two sets of data: one from the measured data and one from the simulated model.

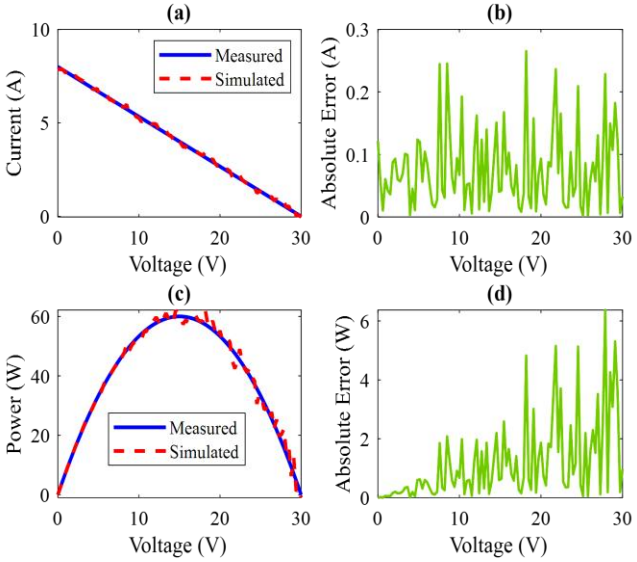

Fig. 11. Absolute error I-V and P-V curve PVCs using MATLAB code. (a) I-V curve. (b) Absolute error in I-V. (c) P-V curve. (d) Absolute error in P-V

Finally, another important aspect of PVCs is the calculation of QE. This technique, which enables the amount of light transmission to particles to be measured as an indicator of the wavelength of hitting light, is crucial for researching PVCs. The amount of particles absorbed by the PVC to photons reflected on the cell at a specific wavelength is known as QE [132]. There are two types of QE: EQE and IQE [133]. Although IQE only takes into account the absorbed photons, EQE is defined as the number of electrons supplied to the external circuit per photon incident on the device; in other words, it is the ratio of the number of charge carriers collected by a device with the number of incident photons. This is why IQE is always greater than EQE [134]. The EQE can be written by formula:

$$EQE = \frac{hc}{nq\lambda}\frac{s(\lambda)}{A} \tag{14}$$

where h is Planck's constant, c is the light speed, λ is the wavelength in nm, $s(\lambda)$ is the spectral sensitivity in AW^{-1}, and n is refraction index [132], [134], [135].

Fig. 12 shows the EQE verses wavelength of solar radiation for different types of PVCs. Fig. 12(a) show the EQE verses wavelength for a Silicon PVC. Peak QE in the visible range is the maximum efficiency with which a given detector, such as a scientific camera sensor (which is made of silicon material), converts incident photons of visible light into electrons, i.e. into a measurable electrical signal. Fig. 12(b) show the EQE verses wavelength for an organic PVC. The peak absorption range of a PVCs is the wavelength range over which it absorbs sunlight most effectively to be as efficient as possible. This is essential for converting solar energy into electricity efficiently. Fig. 12(c) show the EQE verses wavelength for a Perovskite PVC. In general, the High

QE region is the wavelength range over which a given detector has high quantum efficiency. For the Perovskite PVC this range is 450 - 750 nm (Fig. 12(c)). Fig. 12(d) show the EQE verses wavelength for a quantum dot PVC. Strong NIR absorption is the ability of a PVC to efficiently absorb sunlight in the Near Infrared (NIR) area of the electromagnetic spectrum. This spectrum is from 600 nm to 950 nm for a quantum dot PVC.

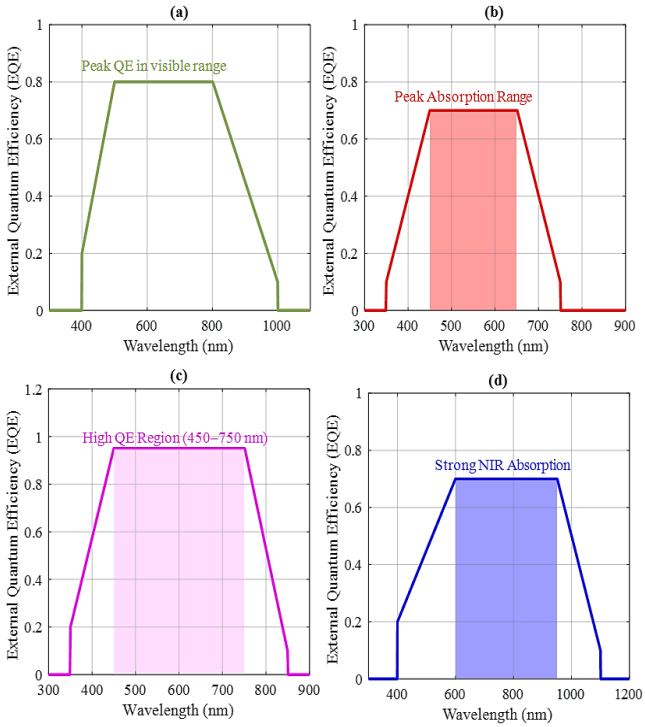

Fig. 12. (a) QE of a silicon PVC. (b) QE of an organic PVC. (c) QE of a perovskite PVC. (d) QE of a quantum dot PVC

IV. CONCLUSIONS

The electrical behavior of PVCs is inherently nonlinear, making the I–V and P–V relationships uplifting in landscape. As such, they cannot be answered methodically in closed form. While analytical techniques offer exact solutions under idealized assumptions, they often fall short when applied to real-world PV models with multiple unknowns and non-ideal parameters. In contrast, numerical methods offer practical and efficient means to approximate the behavior of PVCs, particularly when dealing with nonlinearities. Generally, computer-based modeling is necessary for ray tracing simulation and performance optimization with MATLAB. The simulation results indicated a rise in SR with a constant temperature to enhance the Isc and power harvest, with very little impact on the voltage. On the contrary, increasing temperature would reduce voltage and power while leaving the current relatively unchanged. This again demonstrates that higher temperature leads to lower performance, highlighting the importance of thermal management.

The ideality factor of the diode and I_0 remains essential considerations. An increase in the ideality factor tends to increase the output power. In contrast, the diode saturation current has precisely the opposite effect-an increase in saturation current reduces the output power. Changes in shunt resistance also have a profound impact on performance: the lower the shunt resistance, the lower the output power, implying higher leakage loss within the PVC.

Aside from the electrical characteristics, this study determined the EQE for different PV technologies. The aptitude of a PV to turn episode photons into electrons is quantified by the EQE, which may be assessed as a function of wavelength to obtain the spectral response of silicon PVCs and three other technologies: organic, perovskite, and quantum dot PVCs. A strong EQE response in the visible spectrum indicates good sunlight absorption, whereas EQE drops dramatically at certain wavelengths, which could indicate defects or poor design. These comparisons demonstrate the varying responses to different segments of the solar spectrum of different classes of PV materials. Characteristics in the EQE curves unique to a given cell are related to its structural and compositional design and thus make the analysis of EQE valuable in assessing and selecting materials to enhance solar conversion efficiency.

Overall, the modeling, temperature control, and material optimization aspects of the design and evaluation of PV systems stand validated through this study.

DECLARATIONS

Data Availability Statement: Availability of data and materials Datasets used and/or analyzed during the current study are available from the corresponding author upon reasonable request.

Competing interests: The authors declare no competing interests.

Ethical approval and consent to participate: Not applicable.

Acknowledgment: The authors extend their appreciation to the Northern Border University, Saudi Arabia for supporting this work through project number "NBU-CRP-2025-2448''.

REFERENCES

[1] R. A. Marques Lameirinhas, J. P. N. Torres, and J. P. de Melo Cunha, "A Photovoltaic Technology Review: History, Fundamentals and Applications," *Energies*, vol. 15, no. 5. 2022, doi: 10.3390/en15051823.

[2] H. Abdelfattah, I. Elzein, M. M. Mahmoud, M. I. Mosaad, W. Fendzi Mbasso, and N. F. Ibrahim, "Supporting the reactivity of nuclear power plants using an optimized FOPID controller with arithmetic algorithm: Toward an environmentally sustainable energy system," *Energy Explor. Exploit.*, 2025, doi: 10.1177/01445987251357362.

[3] P. Sinha *et al.*, "Classifying Power Quality Issues in Railway Electrification Systems Using a Nonsubsampled Contourlet Transform Approach," *Eng. Reports*, vol. 7, no. 8, 2025, doi: 10.1002/eng2.70301.

[4] A. O. Ali *et al.*, "Advancements in photovoltaic technology: A comprehensive review of recent advances and future prospects," *Energy Convers. Manag. X*, vol. 26, p. 100952, 2025, doi: 10.1016/j.ecmx.2025.100952.

[5] A. M. El-Rifaie, S. Abid, A. R. Ginidi, and A. M. Shaheen, "Fractional Order PID Controller Based-Neural Network Algorithm for LFC in Multi-Area Power Systems," *Eng. Reports*, vol. 7, no. 2, 2025, doi: 10.1002/eng2.70028.

[6] A. M. Elsayed, A. M. El-Rifaie, M. F. Areed, A. M. Shaheen, and M. O. Atallah, "Allocation and control of multi-devices voltage regulation in distribution systems via rough set theory and grasshopper algorithm: A practical study," *Results Eng.*, vol. 25, p. 103860, 2025, doi: 10.1016/j.rineng.2024.103860.

[7] E. Çelik *et al.*, "Reconfigured single- and double-diode models for improved modelling of solar cells/modules," *Sci. Rep.*, vol. 15, no. 1, pp. 1–19, 2025, doi: 10.1038/s41598-025-86063-2.

[8] E. J. D. Oliva and R. Atehortua Santamaria, "Decoding Solar Adoption: A Systematic Review of Theories and Factors of Photovoltaic Technology Adoption in Households of Developing Countries," *Sustain.*, vol. 17, no. 12, pp. 1–23, 2025, doi: 10.3390/su17125494.

[9] S. Obukhov, A. Ibrahim, M. A. Tolba, and A. M. El-Rifaie, "Power balance management of an autonomous hybrid energy system based on the dual-energy storage," *Energies*, vol. 12, no. 24, 2019, doi: 10.3390/en12244690.

[10] M. Rawa *et al.*, "Single Diode Solar Cells—Improved Model and Exact Current–Voltage Analytical Solution Based on Lambert's W Function," *Sensors*, vol. 22, no. 11, 2022, doi: 10.3390/s22114173.

[11] N. F. Ibrahim *et al.*, "Operation of Grid-Connected PV System with ANN-Based MPPT and an Optimized LCL Filter Using GRG Algorithm for Enhanced Power Quality," *IEEE Access*, vol. 11, pp. 106859–106876, 2023, doi: 10.1109/ACCESS.2023.3317980.

[12] N. F. Ibrahim *et al.*, "A new adaptive MPPT technique using an improved INC algorithm supported by fuzzy self-tuning controller for a grid-linked photovoltaic system," *PLoS One*, vol. 18, no. 11, pp. 1–22, 2023, doi: 10.1371/journal.pone.0293613.

[13] M. S. Priyadarshini, S. A. E. M. Ardjoun, A. Hysa, M. M. Mahmoud, U. Sur, and N. Anwer, "Time-domain Simulation and Stability Analysis of a Photovoltaic Cell Using the Fourth-order Runge-Kutta Method and Lyapunov Stability Analysis," *Bul. Ilm. Sarj. Tek. Elektro*, vol. 7, no. 2, pp. 214–230, 2025, doi: 10.12928/biste.v7i2.13233.

[14] A. Hysa, M. M. Mahmoud, and A. Ewais, "An Investigation of the Output Characteristics of Photovoltaic Cells Using Iterative Techniques and MATLAB ® 2024a Software," *Control Syst. Optim. Lett.*, vol. 3, no. 1, pp. 46–52, 2025, doi: 10.59247/csol.v3i1.174.

[15] S. Basu *et al.*, "Applications of Snow Ablation Optimizer for Sustainable Dynamic Dispatch of Power and Natural Gas Assimilating Multiple Clean Energy Sources," *Eng. Reports*, vol. 7, no. 6, pp. 1–12, 2025, doi: 10.1002/eng2.70211.

[16] M. U. Siddiqui, M. F. Shahab, O. K. Siddiqui, H. Ali, and S. M. Zubair, "A comprehensive multi-physics model of photovoltaic modules with non-uniform solar concentration and serpentine cooling," *Energy Convers. Manag.*, vol. 271, 2022, doi: 10.1016/j.enconman.2022.116266.

[17] S. Murkute and V. A. Kulkarni (Deodhar), "New high performance PV system architecture for mitigation of partial shading effects," *e-Prime - Adv. Electr. Eng. Electron. Energy*, vol. 5, 2023, doi: 10.1016/j.prime.2023.100189.

[18] A. M *et al.*, "Prediction of Optimum Operating Parameters to Enhance the Performance of PEMFC Using Machine Learning Algorithms," *Energy Explor. Exploit.*, 2024, doi: 10.1177/01445987241290535.

[19] T. H. M. Ahmed Tawfik Hassan *et al.*, "Adaptive Load Frequency Control in Microgrids Considering PV Sources and EVs Impacts: Applications of Hybrid Sine Cosine Optimizer and Balloon Effect Identifier Algorithms," *Int. J. Robot. Control Syst.*, vol. 4, no. 2, pp. 941–957, 2024.

[20] T. Boutabba, I. Benlaloui, F. Mechnane, I. M. Elzein, M. Ammar, and M. M. Mahmoud, "Design of a Small Wind Turbine Emulator for Testing Power Converters Using dSPACE 1104," *Int. J. Robot. Control Syst.*, vol. 5, no. 2, pp. 698–712, 2025, doi: 10.31763/ijrcs.v5i2.1685.

[21] P. Mei, H. R. Karimi, C. Huang, F. Chen, and S. Yang, "Remaining driving range prediction for electric vehicles: Key challenges and outlook," *IET Control Theory and Applications*, vol. 17, no. 14. pp. 1875–1893, 2023. doi: 10.1049/cth2.12486.

[22] O. Makram Kamel, I. M. Elzein, M. M. Mahmoud, A. Y. Abdelaziz, M. M. Hussein, and A. A. Zaki Diab, "Effective energy management strategy with a novel design of fuzzy logic and JAYA-based controllers in isolated DC/AC microgrids: A comparative analysis," *Wind Eng.*, vol. 49, no. 1, pp. 199–222, 2025, doi: 10.1177/0309524X241263518.

[23] O. M. Kamel, A. A. Z. Diab, M. M. Mahmoud, A. S. Al-Sumaiti, and H. M. Sultan, "Performance Enhancement of an Islanded Microgrid with the Support of Electrical Vehicle and STATCOM Systems," *Energies*, vol. 16, no. 4, 2023, doi: 10.3390/en16041577.

[24] S. Sachan, S. Deb, and S. N. Singh, "Different charging infrastructures along with smart charging strategies for electric vehicles," *Sustain. Cities Soc.*, vol. 60, 2020, doi: 10.1016/j.scs.2020.102238.

[25] S. Ashfaq *et al.*, "Comparing the Role of Long Duration Energy Storage Technologies for Zero-Carbon Electricity Systems," *IEEE Access*, vol. 12, pp. 73169–73186, 2024, doi: 10.1109/ACCESS.2024.3397918.

[26] A. Maheshwari *et al.*, "Real-Time Parameter Identification and State of Charge Estimation of Electric Vehicle Batteries," *Eng. Reports*, vol. 7, no. 8, 2025, doi: 10.1002/eng2.70346.

[27] F. Menzri *et al.*, "Applications of Novel Combined Controllers for Optimizing Grid-Connected Hybrid Renewable Energy Systems," *Sustain.*, vol. 16, no. 16, 2024, doi: 10.3390/su16166825.

[28] N. Benalia *et al.*, "Enhancing electric vehicle charging performance through series-series topology resonance-coupled wireless power transfer," *PLoS One*, vol. 19, no. 3, 2024, doi: 10.1371/journal.pone.0300550.

[29] C. Sun, T. Li, and X. Tang, "A Data-Driven Approach for Optimizing Early-Stage Electric Vehicle Charging Station Placement," *IEEE Trans. Ind. Informatics*, vol. 20, no. 10, pp. 11500–11510, 2024, doi: 10.1109/TII.2023.3245633.

[30] M. A. Rehman, M. Numan, H. Tahir, U. Rahman, M. W. Khan, and M. Z. Iftikhar, "A comprehensive overview of vehicle to everything (V2X) technology for sustainable EV adoption," *Journal of Energy Storage*, vol. 74. 2023, doi: 10.1016/j.est.2023.109304.

[31] M. M. R. Ahmed *et al.*, "Mitigating Uncertainty Problems of Renewable Energy Resources Through Efficient Integration of Hybrid Solar PV/Wind Systems Into Power Networks," *IEEE Access*, vol. 12, pp. 30311–30328, 2024, doi: 10.1109/ACCESS.2024.3370163.

[32] S. Heroual, B. Belabbas, Y. Diab, M. M. Mahmoud, T. Allaoui, and N. Benabdallah, "Optimizing Power Flow in Photovoltaic-Hybrid Energy Storage Systems: A PSO and DPSO Approach for PI Controller Tuning," *Int. Trans. Electr. Energy Syst.*, vol. 2025, no. 1, 2025, doi: 10.1155/etep/9958218.

[33] J. Zuboy *et al.*, "Getting Ahead of the Curve: Assessment of New Photovoltaic Module Reliability Risks Associated With Projected Technological Changes," *IEEE J. Photovoltaics*, vol. 14, no. 1, pp. 4–22, 2024, doi: 10.1109/JPHOTOV.2023.3334477.

[34] A. E. Magdalin *et al.*, "Development of lead-free perovskite solar cells: Opportunities, challenges, and future technologies," *Results in Engineering*, vol. 20, 2023, doi: 10.1016/j.rineng.2023.101438.

[35] P. Sinha *et al.*, "Efficient automated detection of power quality disturbances using nonsubsampled contourlet transform & PCA-SVM," *Energy Explor. Exploit.*, vol. 43, no. 3, pp. 1149-1179, 2025, doi: 10.1177/01445987241312755.

[36] Y. Chen, M. Zhang, F. Li, and Z. Yang, "Recent Progress in Perovskite Solar Cells: Status and Future," *Coatings*, vol. 13, no. 3, 2023, doi: 10.3390/coatings13030644.

[37] O. Ayadi, R. Shadid, A. Bani-Abdullah, M. Alrbai, M. Abu-Mualla, and N. A. Balah, "Experimental comparison between Monocrystalline, Polycrystalline, and Thin-film solar systems under sunny climatic conditions," *Energy Reports*, vol. 8, pp. 218–230, 2022, doi: 10.1016/j.egyr.2022.06.121.

[38] P. Kumar, S. You, and A. Vomiero, "Recent Progress in Materials and Device Design for Semitransparent Photovoltaic Technologies," *Advanced Energy Materials*, vol. 13, no. 39, 2023, doi: 10.1002/aenm.202301555.

[39] S. R. K. Joga *et al.*, "Applications of tunable-Q factor wavelet transform and AdaBoost classier for identification of high impedance faults: Towards the reliability of electrical distribution systems," *Energy Explor. Exploit.*, vol. 42, no. 6, pp. 2017-2055, 2024, doi: 10.1177/01445987241260949.

[40] J. Liu *et al.*, "Polymer synergy for efficient hole transport in solar cells and photodetectors," *Energy Environ. Sci.*, vol. 16, no. 10, pp. 4474–4485, 2023, doi: 10.1039/d3ee02033a.

[41] B. Krishna Ponukumati *et al.*, "Evolving fault diagnosis scheme for unbalanced distribution network using fast normalized cross-correlation technique," *PLoS One*, vol. 19, no. 10, pp. 1–23, 2024, doi: 10.1371/journal.pone.0305407.

[42] Y. Maamar *et al.*, "A Comparative Analysis of Recent MPPT Algorithms (P & O \ INC \ FLC) for PV Systems," *J. Robot. Control*, vol. 6, no. 4, pp. 1581–1588, 2025, doi: 10.18196/jrc.v6i4.25814.

[43] A. Fatah *et al.*, "Design, and dynamic evaluation of a novel photovoltaic pumping system emulation with DS1104 hardware setup:

Towards innovative in green energy systems," *PLoS One*, vol. 19, no. 10, p. e0308212, 2024, doi: 10.1371/journal.pone.0308212.

[44] S. Heroual, B. Belabbas, and N. B. Elzein I M, Yasser Diab, Alfian Ma'arif, Mohamed Metwally Mahmoud, Tayeb Allaoui, "Enhancement of Transient Stability and Power Quality in Grid-Connected PV Systems Using SMES," *Int. J. Robot. Control Syst.*, vol. 5, no. 2, pp. 990–1005, 2025, doi: 10.31763/ijrcs.v5i2.1760.

[45] A. Alkuhayli, U. Khaled, and M. M. Mahmoud, "A Novel Hybrid Harris Hawk Optimization – Sine Cosine Transmission Network," *Energies, Mdpi*, vol. 17, no. 19, p. 4985, 2024, doi: 10.3390/en17194985.

[46] M. Härtel *et al.*, "Reducing sputter damage-induced recombination losses during deposition of the transparent front-electrode for monolithic perovskite/silicon tandem solar cells," *Sol. Energy Mater. Sol. Cells*, vol. 252, 2023, doi: 10.1016/j.solmat.2023.112180.

[47] S. A. M. Abdelwahab, A. M. El-Rifaie, H. Y. Hegazy, M. A. Tolba, W. I. Mohamed, and M. Mohamed, "Optimal Control and Optimization of Grid-Connected PV and Wind Turbine Hybrid Systems Using Electric Eel Foraging Optimization Algorithms," *Sensors*, vol. 24, no. 7, 2024, doi: 10.3390/s24072354.

[48] G. M. G. Khalaf *et al.*, "Lead Halide Ligand Recycling Enables Low-Cost Infrared PbS Quantum Dot Solar Cells," *ACS Appl. Nano Mater.*, vol. 7, no. 4, pp. 4152–4161, 2024, doi: 10.1021/acsanm.3c05703.

[49] R. Moumni, K. Laroussi, I. Benlaloui, M. M. Mahmoud, and M. F. Elnaggar, "Optimizing Single-Inverter Electric Differential System for Electric Vehicle Propulsion Applications," *Int. J. Robot. Control Syst.*, vol. 4, no. 4, pp. 1772–1793, 2024, doi: 10.31763/ijrcs.v4i4.1542.

[50] Q. Xu, Y. Ji, D. D. Krut, J. H. Ermer, and M. D. Escarra, "Transmissive concentrator multijunction solar cells with over 47% in-band power conversion efficiency," *Appl. Phys. Lett.*, vol. 109, no. 19, 2016, doi: 10.1063/1.4967376.

[51] L. Zaghba, A. Borni, M. Khennane, and A. Fezzani, "Modeling and simulation of novel dynamic control strategy for grid-connected photovoltaic systems under real outdoor weather conditions using Fuzzy–PI MPPT controller," *Int. J. Model. Simul.*, vol. 43, no. 5, pp. 549–558, 2023, doi: 10.1080/02286203.2022.2094663.

[52] A. Rasoulian, H. Saghafi, M. Abbasian, and M. Delshad, "Deep learning based model predictive control of active filter inverter as interface for photovoltaic generation," *IET Renew. Power Gener.*, vol. 17, no. 13, pp. 3151–3162, 2023, doi: 10.1049/rpg2.12822.

[53] H. Abdulla, A. Sleptchenko, and A. Nayfeh, "Photovoltaic systems operation and maintenance: A review and future directions," *Renewable and Sustainable Energy Reviews*, vol. 195, 2024, doi: 10.1016/j.rser.2024.114342.

[54] A. Sharma *et al.*, "Performance investigation of state-of-the-art metaheuristic techniques for parameter extraction of solar cells/module," *Sci. Rep.*, vol. 13, no. 1, 2023, doi: 10.1038/s41598-023-37824-4.

[55] M. M. Elymany, M. A. Enany, and N. A. Elsonbaty, "Hybrid optimized-ANFIS based MPPT for hybrid microgrid using zebra optimization algorithm and artificial gorilla troops optimizer," *Energy Convers. Manag.*, vol. 299, 2024, doi: 10.1016/j.enconman.2023.117809.

[56] X. Liu, X. Chen, and X. Ke, "Based on the difference of Newton's method integrated energy system distributed collaborative optimization," *Front. Energy Res.*, vol. 11, 2023, doi: 10.3389/fenrg.2023.1215786.

[57] M. Rasheed, M. N. Al-Darraji, S. Shihab, A. Rashid, and T. Rashid, "Solar PV Modelling and Parameter Extraction Using Iterative Algorithms," in *Journal of Physics: Conference Series*, vol. 1963, no. 1, p. 012059, 2021, doi: 10.1088/1742-6596/1963/1/012059.

[58] M. A. El-Dabah, R. A. El-Sehiemy, H. M. Hasanien, and B. Saad, "Photovoltaic model parameters identification using Northern Goshawk Optimization algorithm," *Energy*, vol. 262, 2023, doi: 10.1016/j.energy.2022.125522.

[59] A. Ramadan, S. Kamel, M. H. Hassan, T. Khurshaid, and C. Rahmann, "An improved bald eagle search algorithm for parameter estimation of different photovoltaic models," *Processes*, vol. 9, no. 7, 2021, doi: 10.3390/pr9071127.

[60] B. S. Mahmood, N. K. Hussein, M. Aljohani, and M. Qaraad, "A Modified Gradient Search Rule Based on the Quasi-Newton Method and a New Local Search Technique to Improve the Gradient-Based Algorithm: Solar Photovoltaic Parameter Extraction," *Mathematics*, vol. 11, no. 19, 2023, doi: 10.3390/math11194200.

[61] N. A. Muhammad, M. F. N. Tajuddin, A. Azmi, M. N. I. Jamaludin, S. M. Ayob, and T. Sutikno, "Experimental study on modified GOA-MPPT for PV system under mismatch conditions," *Int. J. Power Electron. Drive Syst.*, vol. 15, no. 1, pp. 611–622, 2024, doi: 10.11591/ijpeds.v15.i1.pp611-622.

[62] M. F. Jalil, S. Khatoon, I. Nasiruddin, and R. C. Bansal, "Review of PV array modelling, configuration and MPPT techniques," *Int. J. Model. Simul.*, vol. 42, no. 4, pp. 533–550, 2022, doi: 10.1080/02286203.2021.1938810.

[63] D. S. AbdElminaam, E. H. Houssein, M. Said, D. Oliva, and A. Nabil, "An Efficient Heap-Based Optimizer for Parameters Identification of Modified Photovoltaic Models," *Ain Shams Eng. J.*, vol. 13, no. 5, 2022, doi: 10.1016/j.asej.2022.101728.

[64] J. Montano, A. F. T. Mejia, A. A. R. Muñoz, F. Andrade, O. D. Garzon Rivera, and J. M. Palomeque, "Salp swarm optimization algorithm for estimating the parameters of photovoltaic panels based on the three-diode model," *Electron.*, vol. 10, no. 24, 2021, doi: 10.3390/electronics10243123.

[65] L. Fang and L. Pang, "Improved Newton-Raphson Methods for Solving Nonlinear Equations," *J. Adv. Math.*, vol. 13, no. 5, pp. 7403–7407, 2017, doi: 10.24297/jam.v13i5.6533.

[66] O. K. Ajiboye, C. V. Ochiegbu, E. A. Ofosu, and S. Gyamfi, "A review of hybrid renewable energies optimisation: design, methodologies, and criteria," *International Journal of Sustainable Energy*, vol. 42, no. 1. pp. 648–684, 2023. doi: 10.1080/14786451.2023.2227294.

[67] S. A. Mohamed, N. Anwer, and M. M. Mahmoud, "Solving optimal power flow problem for IEEE-30 bus system using a developed particle swarm optimization method: towards fuel cost minimization," *Int. J. Model. Simul.*, vol. 45, no. 1, pp. 307-320, pp. 1–14, 2023, doi: 10.1080/02286203.2023.2201043.

[68] Y. Wardi, C. Seatzu, J. Cortés, M. Egerstedt, S. Shivam, and I. Buckley, "Tracking control by the Newton–Raphson method with output prediction and controller speedup," *Int. J. Robust Nonlinear Control*, vol. 34, no. 1, pp. 397–422, 2024, doi: 10.1002/rnc.6976.

[69] J. Vysocký, L. Foltyn, D. Brkić, R. Praksová, and P. Praks, "Steady-State Analysis of Electrical Networks in Pandapower Software: Computational Performances of Newton–Raphson, Newton–Raphson with Iwamoto Multiplier, and Gauss– Seidel Methods," *Sustain.*, vol. 14, no. 4, 2022, doi: 10.3390/su14042002.

[70] N. Yadav and S. Singh, "Global convergence of improved Chebyshev-Secant type methods," *J. Anal.*, vol. 32, no. 1, pp. 597–611, 2024, doi: 10.1007/s41478-023-00696-y.

[71] P. C. da Silva, O. P. Ferreira, L. D. Secchin, and G. N. Silva, "Secant-inexact projection algorithms for solving a new class of constrained mixed generalized equations problems," *J. Comput. Appl. Math.*, vol. 440, 2024, doi: 10.1016/j.cam.2023.115638.

[72] X. Liu, L. Cui, Q. Tao, Z. Yi, J. Li, and L. Lu, "Dust deposition mechanism and output characteristics of solar bifacial PV panels," *Environ. Sci. Pollut. Res.*, vol. 30, no. 45, pp. 100937–100949, 2023, doi: 10.1007/s11356-023-29518-1.

[73] D. N. Dang, T. Le Viet, H. Takano, and T. N. Duc, "Estimating parameters of photovoltaic modules based on current–voltage characteristics at operating conditions," *Energy Reports*, vol. 9, pp. 18–26, 2023, doi: 10.1016/j.egyr.2022.10.361.

[74] W. Zhang *et al.*, "A Dual-Feedback Adaptive Clone Selection Algorithm with Golden Sine Search for Parameter Identification of Photovoltaic Models," *IEEE Access*, vol. 12, pp. 20341–20357, 2024, doi: 10.1109/ACCESS.2024.3362059.

[75] R. T. Prabu *et al.*, "The Numerical Algorithms and Optimization Approach Used in Extracting the Parameters of the Single-Diode and Double-Diode Photovoltaic (PV) Models," *Int. J. Photoenergy*, vol. 2022, 2022, doi: 10.1155/2022/5473266.

[76] D. Yousri *et al.*, "Modified Interactive Algorithm Based on Runge Kutta Optimizer for Photovoltaic Modeling: Justification Under Partial Shading and Varied Temperature Conditions," *IEEE Access*, vol. 10, pp. 20793–20815, 2022, doi: 10.1109/ACCESS.2022.3152160.

[77] K. M. Coetzer, A. J. Rix, and P. G. Wiid, "Measurement-Based Nonlinear SPICE-Compatible Photovoltaic Models for Simulating the Effects of Surges and Electromagnetic Interference within Installations," *Energies*, vol. 15, no. 21, 2022, doi:

10.3390/en15218162.

[78] H. Abdelhamid, A. Edris, A. Helmy, and Y. Ismail, "Fast and accurate PV model for SPICE simulation," *J. Comput. Electron.*, vol. 18, no. 1, pp. 260–270, 2019, doi: 10.1007/s10825-018-1266-x.

[79] A. Ramadan, S. Kamel, I. B. M. Taha, and M. Tostado-Véliz, "Parameter estimation of modified double-diode and triple-diode photovoltaic models based on wild horse optimizer," *Electron.*, vol. 10, no. 18, 2021, doi: 10.3390/electronics10182308.

[80] H. Bakır, "Comparative performance analysis of metaheuristic search algorithms in parameter extraction for various solar cell models," *Environ. Challenges*, vol. 11, 2023, doi: 10.1016/j.envc.2023.100720.

[81] E. V. H. Udoka, K. U. Umaru, E. Edozie, R. Nafuna, and N. Yudaya, "The Differences between Single Diode Model and Double Diode Models of a Solar Photovoltaic Cells: Systematic Review," *J. Eng. Technol. Appl. Sci.*, vol. 5, no. 2, pp. 57–66, 2023, doi: 10.36079/lamintang.jetas-0502.541.

[82] R. Abbassi, S. Saidi, S. Urooj, B. N. Alhasnawi, M. A. Alawad, and M. Premkumar, "An Accurate Metaheuristic Mountain Gazelle Optimizer for Parameter Estimation of Single- and Double-Diode Photovoltaic Cell Models," *Mathematics*, vol. 11, no. 22, 2023, doi: 10.3390/math11224565.

[83] D. B. Aeggegn, T. F. Agajie, Y. G. Workie, B. Khan, and A. Fopah-Lele, "Feasibility and techno-economic analysis of PV-battery priority grid tie system with diesel resilience: A case study," *Heliyon*, vol. 9, no. 9, 2023, doi: 10.1016/j.heliyon.2023.e19387.

[84] M. Balasubramonian, R. Ramachandran, V. Veerasamy, P. A. C. P. Albert, and N. I. A. Wahab, "A comprehensive analysis of numerical techniques for estimation of solar PV parameters under dynamic environmental condition," in *Smart Grids and Microgrids: Technology Evolution*, pp. 1–26, 2022, doi: 10.1002/9781119760597.ch1.

[85] M. Lakshmanan, C. Kumar, and J. S. Jasper, "Optimal parameter characterization of an enhanced mathematical model of solar photovoltaic cell/module using an improved white shark optimization algorithm," *Optim. Control Appl. Methods*, vol. 44, no. 5, pp. 2374–2425, 2023, doi: 10.1002/oca.2984.

[86] M. Kikelj, B. Lipovšek, M. Bokalič, and M. Topič, "Spatially resolved electrical modelling of cracks and other inhomogeneities in crystalline silicon solar cells," *Prog. Photovoltaics Res. Appl.*, vol. 29, no. 1, pp. 124–133, 2021, doi: 10.1002/pip.3348.

[87] H. Braun *et al.*, "Topology reconfiguration for optimization of photovoltaic array output," *Sustain. Energy, Grids Networks*, vol. 6, pp. 58–69, 2016, doi: 10.1016/j.segan.2016.01.003.

[88] N. Belhaouas, M. S. Ait Cheikh, A. Malek, and C. Larbes, "Matlab-Simulink of photovoltaic system based on a two-diode model simulator with shaded solar cells," *J. Renew. Energies*, vol. 16, no. 1, 2023, doi: 10.54966/jreen.v16i1.364.

[89] G. Barone *et al.*, "Modelling and simulation of building integrated Concentrating Photovoltaic/Thermal Glazing (CoPVTG) systems: Comprehensive energy and economic analysis," *Renew. Energy*, vol. 193, pp. 1121–1131, 2022, doi: 10.1016/j.renene.2022.04.119.

[90] D. S. Lee and S. Y. Son, "PV Forecasting Model Development and Impact Assessment via Imputation of Missing PV Power Data," *IEEE Access*, vol. 12, pp. 12843–12852, 2024, doi: 10.1109/ACCESS.2024.3352038.

[91] S. R. Shakeel, J. K. Juntunen, and A. Rajala, "Business models for enhanced solar photovoltaic (PV) adoption: Transforming customer interaction and engagement practices," *Sol. Energy*, vol. 268, 2024, doi: 10.1016/j.solener.2024.112324.

[92] M. Wang, J. Peng, Y. Luo, Z. Shen, and H. Yang, "Comparison of different simplistic prediction models for forecasting PV power output: Assessment with experimental measurements," *Energy*, vol. 224, 2021, doi: 10.1016/j.energy.2021.120162.

[93] O. Hassan, N. Zakzouk, and A. Abdelsalam, "Novel Photovoltaic Empirical Mathematical Model Based on Function Representation of Captured Figures from Commercial Panels Datasheet," *Mathematics*, vol. 10, no. 3, 2022, doi: 10.3390/math10030476.

[94] M. H. Qais and S. M. Muyeen, "A Novel Adaptive Filtering Algorithm Based Parameter Estimation Technique for Photovoltaic System," *IEEE Trans. Energy Convers.*, vol. 37, no. 1, pp. 286–294, 2022, doi: 10.1109/TEC.2021.3090943.

[95] A. Chauhan and S. Prakash, "Parameter Estimation and Analysis of Photovoltaics through a Hybrid Emperor Penguin Optimisation Approach under Different Environmental Constraints," *IETE J. Res.*, vol. 69, no. 7, pp. 4721–4737, 2023, doi: 10.1080/03772063.2021.1951378.

[96] A. Chauhan and S. Prakash, "A new emperor penguin optimisation-based approach for solar photovoltaic parameter estimation," *Int. Trans. Electr. Energy Syst.*, vol. 31, no. 7, 2021, doi: 10.1002/2050-7038.12917.

[97] S. Lidaighbi, M. Elyaqouti, D. Ben Hmamou, D. Saadaoui, K. Assalaou, and E. Arjdal, "A new hybrid method to estimate the single-diode model parameters of solar photovoltaic panel," *Energy Convers. Manag. X*, vol. 15, 2022, doi: 10.1016/j.ecmx.2022.100234.

[98] P. Hao and Y. Zhang, "An Improved Method for Parameter Identification and Performance Estimation of PV Modules from Manufacturer Datasheet Based on Temperature-Dependent Single-Diode Model," *IEEE J. Photovoltaics*, vol. 11, no. 6, pp. 1446–1457, 2021, doi: 10.1109/JPHOTOV.2021.3114592.

[99] P. Sharma, S. Raju, R. Salgotra, and A. H. Gandomi, "Parametric estimation of photovoltaic systems using a new multi-hybrid evolutionary algorithm," *Energy Reports*, vol. 10, pp. 4447–4464, 2023, doi: 10.1016/j.egyr.2023.11.012.

[100] N. Hamid, M. Elyaqouti, N. Boulfaf, M. Feddaoui, and D. Agliz, "Modelling and characterisation of photovoltaic modules using iterative and analytical methods," *Int. J. Ambient Energy*, vol. 43, no. 1, pp. 5917–5938, 2022, doi: 10.1080/01430750.2021.1997809.

[101] W. L. Lo, H. S. H. Chung, R. T. C. Hsung, H. Fu, and T. W. Shen, "PV Panel Model Parameter Estimation by Using Neural Network," *Sensors*, vol. 23, no. 7, 2023, doi: 10.3390/s23073657.

[102] A. A. Z. DIab, H. M. Sultan, T. D. Do, O. M. Kamel, and M. A. Mossa, "Coyote Optimization Algorithm for Parameters Estimation of Various Models of Solar Cells and PV Modules," *IEEE Access*, vol. 8, pp. 111102–111140, 2020, doi: 10.1109/ACCESS.2020.3000770.

[103] U. Chauhan, H. Chhabra, P. Jain, A. Dev, N. Chauhan, and B. Kumar, "Chaos inspired invasive weed optimization algorithm for parameter estimation of solar PV models," *IFAC J. Syst. Control*, vol. 27, 2024, doi: 10.1016/j.ifacsc.2023.100239.

[104] Q. Liu *et al.*, "Multi-strategy adaptive guidance differential evolution algorithm using fitness-distance balance and opposition-based learning for constrained global optimization of photovoltaic cells and modules," *Appl. Energy*, vol. 353, 2024, doi: 10.1016/j.apenergy.2023.122032.

[105] P. Pandian, P. W. David, P. Murugesan, and P. Murugesan, "Performance Analysis of Novel Solar PV Array Configurations with Reduced Tie Interconnection to Extract Maximum Power under Partial Shading," *Electr. Power Components Syst.*, pp. 1-25, 2023, doi: 10.1080/15325008.2023.2280115.

[106] S. B. Prakash, G. Singh, and S. Singh, "Modeling and Performance Analysis of Simplified Two-Diode Model of Photovoltaic Cells," *Front. Phys.*, vol. 9, 2021, doi: 10.3389/fphy.2021.690588.

[107] H. Kraiem *et al.*, "Parameters Identification of Photovoltaic Cell and Module Models Using Modified Social Group Optimization Algorithm," *Sustain.*, vol. 15, no. 13, 2023, doi: 10.3390/su151310510.

[108] R. Ndegwa, J. Simiyu, E. Ayieta, and N. Odero, "A Fast and Accurate Analytical Method for Parameter Determination of a Photovoltaic System Based on Manufacturer's Data," *J. Renew. Energy*, vol. 2020, pp. 1–18, 2020, doi: 10.1155/2020/7580279.

[109] S. W. Yufenyuy, G. M. Mengata, and L. Nneme Nneme, "Influence of the nature of lamp on model parameters of PV modules operating in an indoor environment," *Energy Reports*, vol. 10, pp. 4374–4388, 2023, doi: 10.1016/j.egyr.2023.10.072.

[110] B. K. Atay and U. Eminoğlu, "A new approach for parameter estimation of the single-diode model for photovoltaic cells/modules," *Turkish J. Electr. Eng. Comput. Sci.*, vol. 27, no. 4, pp. 3026–3039, 2019, doi: 10.3906/elk-1805-161.

[111] D. Ben hmamou *et al.*, "Experimental characterization of photovoltaic systems using sensors based on MicroLab card: Design, implementation, and modeling," *Renew. Energy*, vol. 223, 2024, doi: 10.1016/j.renene.2024.120049.

[112] İ. Çetinbaş, B. Tamyurek, and M. Demirtaş, "Parameter extraction of photovoltaic cells and modules by hybrid white shark optimizer and artificial rabbits optimization," *Energy Convers. Manag.*, vol. 296, 2023, doi: 10.1016/j.enconman.2023.117621.

[113] M. Malvoni and Y. Chaibi, "Machine learning based approaches for modeling the output power of photovoltaic array in real outdoor

conditions," *Electron.*, vol. 9, no. 2, 2020, doi: 10.3390/electronics9020315.

[114] N. Priyadarshi, P. Sanjeevikumar, M. S. Bhaskar, F. Azam, and S. M. Muyeen, "An improved standalone photovoltaic system with hybrid dual integral sliding mode and model predictive control for MPPT," *IET Renew. Power Gener.*, vol. 19, no. 1, 2025, doi: 10.1049/rpg2.12665.

[115] H. H. Ali, M. Ebeed, A. Fathy, F. Jurado, T. S. Babu, and A. A. Mahmoud, "A New Hybrid Multi-Population GTO-BWO Approach for Parameter Estimation of Photovoltaic Cells and Modules," *Sustain.*, vol. 15, no. 14, 2023, doi: 10.3390/su151411089.

[116] O. S. Elazab, H. M. Hasanien, I. Alsaidan, A. Y. Abdelaziz, and S. M. Muyeen, "Parameter estimation of three diode photovoltaic model using grasshopper optimization algorithm," *Energies*, vol. 13, no. 2, 2020, doi: 10.3390/en13020497.

[117] R. Castro and M. Silva, "Experimental and theoretical validation of one diode and three parameters–based pv models," *Energies*, vol. 14, no. 8, 2021, doi: 10.3390/en14082140.

[118] H. Shaban *et al.*, "Identification of parameters in photovoltaic models through a runge kutta optimizer," *Mathematics*, vol. 9, no. 18, 2021, doi: 10.3390/math9182313.

[119] Z. Duan, H. Yu, Q. Zhang, and L. Tian, "Parameter Extraction of Solar Photovoltaic Model Based on Nutcracker Optimization Algorithm," *Appl. Sci.*, vol. 13, no. 11, 2023, doi: 10.3390/app13116710.

[120] N. Kullampalayam Murugaiyan, K. Chandrasekaran, P. Manoharan, and B. Derebew, "Leveraging opposition-based learning for solar photovoltaic model parameter estimation with exponential distribution optimization algorithm," *Sci. Rep.*, vol. 14, no. 1, 2024, doi: 10.1038/s41598-023-50890-y.

[121] K. Tifidat, N. Maouhoub, S. S. Askar, and M. Abouhawwash, "Numerical procedure for accurate simulation of photovoltaic modules performance based on the identification of the single-diode model parameters," *Energy Reports*, vol. 9, pp. 5532–5544, 2023, doi: 10.1016/j.egyr.2023.04.378.

[122] S. Song, P. Wang, A. A. Heidari, X. Zhao, and H. Chen, "Adaptive Harris hawks optimization with persistent trigonometric differences for photovoltaic model parameter extraction," *Eng. Appl. Artif. Intell.*, vol. 109, 2022, doi: 10.1016/j.engappai.2021.104608.

[123] M. Ćalasan, S. H. E. Abdel Aleem, and A. F. Zobaa, "On the root mean square error (RMSE) calculation for parameter estimation of photovoltaic models: A novel exact analytical solution based on Lambert W function," *Energy Convers. Manag.*, vol. 210, 2020, doi: 10.1016/j.enconman.2020.112716.

[124] H. M. Ridha, H. Hizam, S. Mirjalili, M. L. Othman, and M. E. Ya'acob, "Zero root-mean-square error for single- and double-diode photovoltaic models parameter determination," *Neural Comput. Appl.*, vol. 34, no. 14, pp. 11603–11624, 2022, doi: 10.1007/s00521-022-07047-1.

[125] G. Karthikeyan and A. Jagadeeshwaran, "Enhancing Solar Energy Generation: A Comprehensive Machine Learning-Based PV Prediction and Fault Analysis System for Real-Time Tracking and Forecasting," *Electr. Power Components Syst.*, vol. 52, no. 9, pp. 1497–1512, 2024, doi: 10.1080/15325008.2023.2293947.

[126] K. Lappalainen, M. Piliougine, and G. Spagnuolo, "Experimental comparison between various fitting approaches based on RMSE minimization for photovoltaic module parametric identification," *Energy Convers. Manag.*, vol. 258, 2022, doi: 10.1016/j.enconman.2022.115526.

[127] G. Badran and M. Dhimish, "A comparative study of bifacial versus monofacial PV systems at the UK's largest solar plant," *Clean Energy*, vol. 8, no. 4, pp. 248–260, 2024, doi: 10.1093/ce/zkae043.

[128] D. S. Braga, L. L. Kazmerski, D. A. Cassini, V. Camatta, and A. S. A. C. Diniz, "Performance of bifacial PV modules under different operating conditions in the State of Minas Gerais, Brazil," *Renew. Energy Environ. Sustain.*, vol. 8, p. 23, 2023, doi: 10.1051/rees/2023021.

[129] K. Ganesan, D. P. Winston, J. J. D. Nesamalar, and M. Pravin, "Output power enhancement of a bifacial solar photovoltaic with upside down installation during module defects," *Appl. Energy*, vol. 353, 2024, doi: 10.1016/j.apenergy.2023.122070.

[130] M. Dhimish and G. Badran, "Investigating defects and annual degradation in UK solar PV installations through thermographic and electroluminescent surveys," *npj Mater. Degrad.*, vol. 7, no. 1, 2023, doi: 10.1038/s41529-023-00331-y.

[131] D. A. Rodriguez-Pastor, A. F. Ildefonso-Sanchez, V. M. Soltero, M. E. Peralta, and R. Chacartegui, "A new predictive model for the design and evaluation of bifacial photovoltaic plants under the influence of vegetation soils," *J. Clean. Prod.*, vol. 385, 2023, doi: 10.1016/j.jclepro.2022.135701.

[132] A. M. Karmalawi, D. A. Rayan, and M. M. Rashad, "Establishment and evaluation of photovoltaic quantum efficiency system at central metallurgical research and development institute," *Optik (Stuttg).*, vol. 217, 2020, doi: 10.1016/j.ijleo.2020.164931.

[133] S. E. Shaheen, C. J. Brabec, N. S. Sariciftci, F. Padinger, T. Fromherz, and J. C. Hummelen, "2.5% efficient organic plastic solar cells," *Appl. Phys. Lett.*, vol. 78, no. 6, pp. 841–843, 2001, doi: 10.1063/1.1345834.

[134] K. Ramakrishnan, B. Ajitha, and Y. Ashok Kumar Reddy, "Review on metal sulfide-based nanostructures for photodetectors: From ultraviolet to infrared regions," *Sensors and Actuators A: Physical*, vol. 349, 2023, doi: 10.1016/j.sna.2022.114051.

[135] N. Ali *et al.*, "Beyond lead: Progress in stable and non-toxic lower-dimensional perovskites for high-performance photodetection," *Sustainable Materials and Technologies*, vol. 38, 2023, doi: 10.1016/j.susmat.2023.e00759.